Errors in Calculating Solar Heating of the Climate System

Juno C. Hsu[1], Michael J. Prather[1]

[1]Department of Earth System Science, University of California, Irvine, CA, USA

Corresponding author: Juno Hsu (junoh@uci.edu)

Key Points:

- Summarize 12 common errors in community solar heating codes used for climate simulations, and quantify 10 of them
- Find that cloud absorption spectral resolution, ice cloud parameterization, and cloud overlap schemes are large error sources and require new research
- Show other significant error sources can be minimized by adapting modern radiative transfer techniques, such as used in the Solar-J code here

Abstract

In calculating solar radiation, climate models make many approximations to the known physics of radiative transfer. These simplifying parameterizations are made to reduce computational cost and enable climate modeling, but they obviously cause errors in solar heating that impact the simulated climate. Most of these radiative transfer errors have been identified individually in isolated examples, but here we quantify them in terms of net solar heating of the atmosphere and surface within a consistent framework on a scale relevant to the global climate. We build a benchmark capability around a solar heating code (Solar-J) that already includes some of the more accurate radiative transfer methods and add further improvements covering known errors. The error classes assessed here include: use of broad wavelength bins to integrate over fine spectral features; multiple-scattering approximations that alter the scattering phase function and optical depth for clouds, aerosols, and gases; uncertainty in ice-cloud optics; treatment of fractional cloud cover including cloud overlap; and constant ocean surface albedo. We geographically map the errors in terms of W m^{-2} using a full climate re-creation for January 2015 from weather forecasting models. For many of the ten specific approximations calculated here, the mean errors are ~2 W m^{-2} with even larger latitudinal biases and are likely to affect a model's ability to match the current climate state. From this study, we are able to make priority recommendations for these errors, pointing out where codes can be simply updated and where more scientific development is needed.

Plain Language Summary

Solar heating of the climate system-- the atmosphere, land surface, and ocean--drives the climate. Accurate numerical calculation of solar heating is a core component of the models we use to project and prepare for climate change. Radiative transfer is a classic science, and we know how to calculate solar heating accurately, but the large computational cost of these more accurate solutions means that we make many approximations to the radiative transfer calculations in our current climate models. Systematic errors, or biases, may not affect the calculated change in climate now being forced by greenhouse gases, but they may push a model's baseline current climate into a pre-industrial or future climate regime. This paper examines ten well known approximations in use, quantifies them in context of the climate system, and then recommends a number of cheap and easy fixes, assessment of the more costly but fixable problems, and areas where new research is needed.

1. Introduction

The heat from sunlight drives the weather and climate system, the energy in solar photons drives atmospheric chemistry, and the photosynthetically active radiation drives life. For Earth system models (ESMs), one needs to calculate the scattering, absorption, and reflection of solar radiation throughout the atmosphere, ocean, cryosphere, and land surface. This radiative transfer (RT) problem is well known and in many cases has near-exact, but costly solutions. Thus, solar heating calculations in ESMs use numerous approximations with manifold potential for errors. Here, we systematically examine many of these approximations using a more costly and accurate RT code as a benchmark to assess the errors in current solar heating models.

We evaluate the approximation errors in solar energy under realistic meteorology for the Earth in January 2015 using modified versions of the Solar-J code (Prather & Hsu, 2019, hence P2019; Hsu et al, 2017; hence H2017). The errors are mapped geographically in W m^{-2} for the primary components: incident, reflected, absorbed in the atmosphere (troposphere vs upper atmosphere), and absorbed at the surface. For most cases, we find that global mean absolute errors range from 0.5 to 5 W m^{-2} with much larger systematic latitudinal or root-mean-square errors. Such error levels are likely to shift ESMs to different climate regimes for the current reference period (e.g., 1980-2010) as they are comparable to the changes in climate forcing by greenhouse gases from pre-industrial to present (Myhre et al., 2013). Many of these error-prone approximations could be fixed with minimal effort or cost, but others might impose excessive computational costs for extensive climate simulations.

The errors caused by ignoring spherical geometry have been analyzed recently in P2019. In this paper we examine different classes of errors: the use of broad wavelength bins to integrate over fine spectral features (Section 2); multiple-scattering approximations that alter the scattering phase function for clouds, aerosols, and gases (Section 3); uncertainty in ice-cloud optics (Section 4); treatment of fractional cloud cover including cloud overlap (Section 5); and approximation of ocean surface albedo as a constant (Section 6). Where a current method is compared with a more accurate, physically based method, we can quantify errors to first order; but when two methods choose different approaches that might be equally valid; we can quantify differences that highlight uncertainty in our methods. In many cases these approximations are evaluated using a modified version of Solar-J which uses the same long-wavelength (>700 nm) spectral code as RRTMG (Clough et al., 2005); but in others, we compare by running the publicly available RRTMG-SW version 4.0 in parallel with Solar-J. A major approximation not covered here is that of 1D plane-parallel radiative transfer: we assume that vertical profiles of clouds, aerosols, ozone and water vapor are horizontally uniform. The impact of a spherical atmosphere on the incidence flux is assessed in P2019, and so most of the comparisons here are made with a flat atmosphere for consistency with other solar heating codes. Section 7 reviews the RT approximations evaluated here and makes priority recommendations for fixes for 12 of the resulting errors, pointing out where more scientific development is needed.

2. Wavelength binning

Practical RT solutions for the complex absorption features of atmospheric gases require selecting a limited number of wavelength intervals (bins) for the calculation. Ideally, one picks as wide an interval as possible that has nearly constant absorption features so that the attenuation of sunlight is nearly the same across all wavelengths in that bin. For example, in the wavelength region from 233 nm to 276 nm, ozone is the only important absorber and its cross section is changing very slowly, so that a single RT calculation accurately represents all wavelengths in the 233-276 nm bin. In wavelength regions with many absorption lines, such as the Schumann-Runge bands of O_2 (177 – 200 nm), the opacity distribution method (Fang et al., 1974) sorts the lines to get sub-bins of individual wavelengths with about the same opacity, effectively collecting a set of non-continuous intervals with similar opacity. For solar absorption in the infrared, a similar method is called correlated-k (Lacis & Oinas, 1991). The art here lies in selecting the minimum number of bins and sub-bins that still reproduce the result from spectrally resolved models using thousands of wavelength intervals.

Fast-J optimized the wavelength bins for solar RT in the ultraviolet and visible regions (Bian & Prather, 2002; Wild et al., 2000) and builds upon four decades of RT development for atmospheric chemistry (Logan et al., 1978). Solar-J retains that bin structure. For wavelengths >500 nm, Solar-J was configured to run with flexible wavelength bins (Hsu et al., 2017). The standard operational version (H2017), denoted simply *SJ*, is derived from RRTMG-SW version 4.0 (Clough et al., 2005; Mlawer et al., 1997) with 9 large infrared bins (0.78 – 12.2 μm) and with 78 sub-bins for infrared gas absorption (also denoted g-bins in RRTM notation). The most accurate Solar-J version in terms of infrared gas absorption is derived from the benchmark code RRTM-SW with the same 9 infrared bins, but 144 sub-bins, denoted *SJ/RRX*. Other, less accurate models include only H_2O-gas absorption in the infrared: CLIRAD (Chou & Suarez, 1996) has 3 large bins (0.70 – 10.0 μm) including 30 sub-bins (denoted *SJ/CLIRAD*); and LLNL (Grant & Grossman, 1998) has 3 large bins (0.69 – 3.85 μm) including 21 sub-bins (denoted *SJ/LLNL*). The accuracy and computational cost increase with the number of infrared sub-bins. The bins have a single set of optical properties for clouds and aerosols that is applied to each sub-bin. We compare the effect of increased sub-bins by running the different versions of Solar-J with H_2O-gas absorption and clear skies (see **Figure 1(left)**). Compared to the standard *SJ*, *SJ/CLIRAD* and *SJ/LLNL* have about 6-8 W m^{-2} less atmospheric absorption, most of which is absorbed at the surface with small fraction (~1 W m^{-2}) being reflected (see ***Table 1 / Rows 1&2***, hence designated ***T1/R1&2***). The more accurate *SJ/RRX* code is nearly identical to *SJ*, with only ~¼ W m^{-2} less atmospheric absorption (***T1/R3***).

The Solar-J *SJ* code, even though it is based on the RRTMG spectral model, has differences relative to full RRTMG-SW version 4.0 code that are caused by different binning in the visible range 300-778 nm and therefore different mixtures of ozone absorption and Rayleigh scattering. For wavelengths > 778 nm, we can verify that both codes are essentially identical under clear-sky conditions. The global mean differences for RRTMG minus SJ under clear sky are [+1.3, -0.5, -0.8 W m^{-2}] for the 3 primary components [reflection, atmospheric absorption, and surface absorption], respectively (***T1/R4***). We believe that Solar-J should be more accurate because RRTMG has 4 bins in this range and Solar-J has 7; however, a super-resolved set of bins (~0.01 nm) could easily establish the best way to select the 300-778 nm bins.

The accuracy of the calculated cloud absorption is determined by the number of infrared bins, not sub-bins. **Figure 2(left)** shows the single-scattering albedo (SSA) of typical ice- and liquid-water clouds over the infrared spectrum. The refractive indices for ice and liquid water are similar but with distinct wavelength shifts: the second deep SSA minimum for liquid occurs about 1.9 μm, while that for ice occurs about 2.0 μm. The largest differences in the liquid vs. ice curves here are caused by particle size, with smaller particles having larger SSA. For the same amount of mass, both small and large particles have about the same absorption optical depth, but the small particles have greater scattering optical depth and hence greater SSA. The 9 infrared bins (#19–#27 in the figure) of RRTMG (and the benchmark code RRTM) are denoted with the vertical dashed lines, and the average cloud single-scattering albedo (SSA) in each bin is shown by the horizontal bar with a circle. A super-cloud-resolving version of Solar-J (denoted *SJ/66b*) was constructed using 0.05 to 0.10 μm wide bins, yielding 66 infrared bins (black squares). *SJ/66b*, without sub-bins, cannot calculate H_2O-gas absorption.

The problem with the RRTM binning is that bins 21-27 average over both reflecting and absorbing wavelengths in clouds. The average SSA can be correct, but calculating cloud heating with an average of high and low SSA leads to a greater fraction of sunlight being absorbed in the top of the cloud. Cloud heating rate profiles in **Figure 2(right)** are calculated with *SJ/66b* and *SJ*, both without infrared gas absorption but retaining O_3 and O_2 absorption in the ultraviolet and visible range which both models can do. *SJ* clearly overestimates cloud-top heating rates. For stratus clouds, the excess heating ranges from +5% (bottom) to +25% (top), with similar values for cirrus clouds. At the top of a stratus cloud, *SJ/66b* heating rates are 1.8 K per day, while *SJ* calculates 2.3 K per day (both are without IR gas absorption). When we add IR gas absorption, we find that heating rates in the upper layers of the stratus cloud are reduced by about 40% because that energy is absorbed by water vapor above the cloud deck. The relative (%) differences between 9 bins and 66 bins should remain. Such solar heating errors are likely to affect the lifetime and stability of clouds (Wood, 2012). In terms of global zonal-mean heating rates (**Figure 1(right)**), *SJ* (no IR gas) has 1.7 W m^{-2} more in-cloud heating than *SJ/66b*, while *SJ/CLIRAD* has 3.8 W m^{-2} more (***T1/R6&7***). Coarse wavelength resolution of cloud absorption clearly results in more in-cloud heating balanced almost equally by less reflection and surface absorption. Improving the accuracy of the gaseous absorption is an ongoing effort (Mlawer et al., 2012; Paynter & Ramaswamy, 2014; Pincus et al., 2015; Etminan et al., 2016), but no parallel effort addresses cloud absorption.

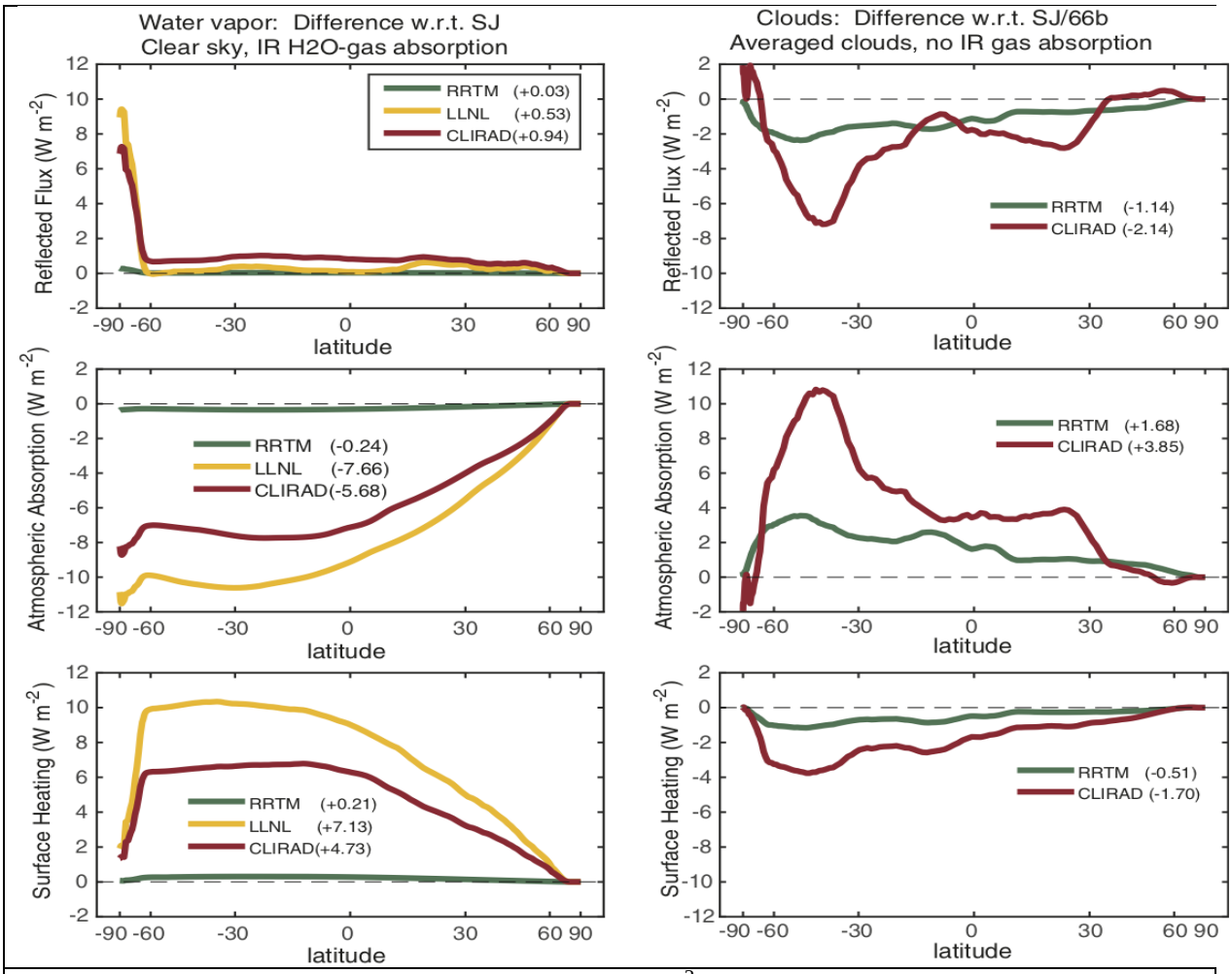

Figure 1 Monthly zonal mean flux differences (W m^{-2}) as a function of latitude for January 2015. The three vertical panels show: reflected, atmospheric and surface absorption, respectively. (left column) Case for H_2O-gas absorption and clear sky emphasizes the number of infrared sub-bins. Differences are relative to standard Solar-J (SJ). RRTM refers to the very high-resolution (SJ/RRX in Table S1); CLIRAD and LLNL, to the courser resolutions (SJ/CLIRAD and SJ/LLNL). (right column) All sky with averaged clouds and no infrared gas absorption, emphasizing the number of infrared bins. Differences are relative to SJ-66b (high-resolution infrared bins for clouds). Both RRTM codes have the same 9 infrared bins, and CLIRAD has 3 infrared bins. See Table S1 for a complete description of code versions.

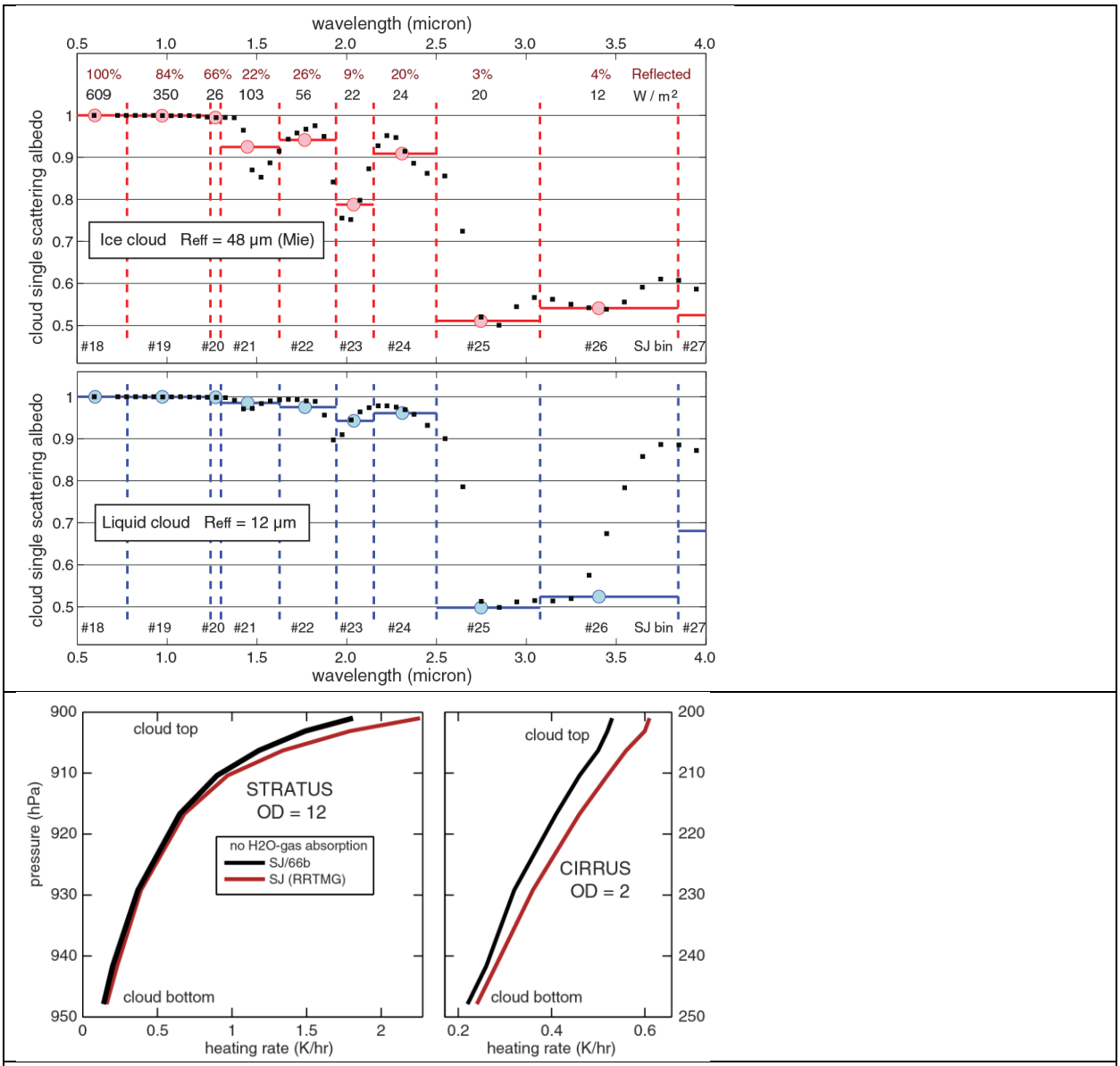

Figure 2. (top panels) Single scattering albedo (SSA, dimensionless) for water clouds versus wavelength (μm), including both ice (top) and liquid water (bottom). The RRTMG infrared bins, designated #18 through #27 are demarcated by dashed vertical lines with average SSA denoted (large circle with cross bar and light-colored fill). The solar energy (W m^{-2}) in each bin is denoted, and the reflected flux (%) for overhead sun and an optically thick ice-water cloud is also given. Average SSA is calculated from a flux-weighted refractive index for each bin assuming spherical (Mie) particles, even for ice-water. The liquid particles have an effective radius of 12 μm; and the ice particles, 48 μm. The black squares show results from the high-resolution SJ-66b, where the resolution ranges from 0.05 μm (0.7 to 2.4 μm) to 0.10 μm (2.5 μm to 4.0 μm). The solar flux (W/m^2) in each RRTM bin is noted in the upper (ice) panel, and the % reflected from an optically thick ice cloud for overhead sun is given above the flux (red). **(bottom)** Profile of in-cloud rates for stratus (optical depth OD=12, liquid water) and cirrus (OD = 2, ice water) from standard 27-bin Solar-J (red) and the 85-bin SJ85b (black) for overhead sun. Water vapor IR absorption is shut off.

181

3. Scattering phase functions and multiple scattering

Ideally, the sunlight scattered by clouds, aerosols and gases is resolved semi-continuously in all directions within the atmosphere, but in practice, RT solutions for solar heating keep track of a limited number of angles (streams) in upward and downward directions and average over the azimuth angle. Solar-J uses 8 streams (4 up, 4 down) to resolve multiple scattering and this RT solution is implemented in many global chemistry models (Prather, 2015). RRTM (Mlawer et al., 1997) uses 16-stream scattering but is not implemented in global models; instead, RRTMG (Clough et al., 2005) with 2-stream scattering is used in many climate models. The GFDL AM3, with 4-stream RT (Li & Ramaswamy, 1996), appears to be the most accurate scattering code currently used for solar heating by climate models.

The number of scattering angles determines how well the scattering phase function, $P(\Theta)$, is resolved, where Θ is the angle between incident and scattered light. Nominally, these phase functions are calculated using Mie theory for spherical droplets or else other approximation for aspherical ice or dust particles (Mishchenko et al., 2016; Yang et al., 2018). M-stream RT methods can use the first M terms in the expansion of Legendre polynomials, $P_m(\Theta)$, where the first term is $P_0 \equiv 1$ (See **Table 2** for the Mie phase function for liquid clouds expanded in terms of coefficients g_m). Modifications to these g coefficients exist (delta-M scaling methods: Lin et al., 2018; Wiscombe, 1977) and are necessary in 2-stream RT. The 8-stream in Solar-J does not use delta-M scaling because early tests showed that simple truncation at the 8^{th} term in the Legendre series compared well to a 160-stream solution for optically thick clouds, with mean intensity differences of 1% throughout most of the atmosphere, and at worst case, 8% in the uppermost layers of a cloud with overhead sun (Wild et al., 2000; see also Wiscombe, 1977).

The phase function for clouds and aerosols is anisotropic with a strong forward-scattering peak. Often, only the first term in the Legendre expansion is calculated and then the simplified analytic Henyey-Greenstein (HG) function is used for the higher-order terms (Boucher, 1998), $P_{HG}(\Theta) = 1 + \Sigma_{m=1:M-1} (2m + 1) (g_1)^m P_m(\cos(\Theta))$. For liquid water clouds, the HG function has serious errors: it lacks the strong forward-scattering peak as well as the back-scatter peak, consequently it is more isotropic and scatters too much at right angles (e.g., see Fig. 1 of Wiscombe, 1977). A version *SJ/HG* has been coded that rewrites the 8-term cloud scattering phase function in each grid cell using Mie value for g_1 and the formula above.

Two-stream methods can directly use only the first two terms in the expansion, $P(\Theta) = 1 + 3\, g^* \cos(\Theta)$, where g^* is the asymmetry parameter. There are various methods for selecting g^* and rescaling the scattering optical depth τ_{sca}. The reduction in cloud optical depth is intended to account for the forward-scattering peak acting as a Dirac delta function, i.e., not a scatter. It applies only to the scattering optical depth τ_{sca}; while the absorbing τ_{abs} is unchanged. Delta-Eddington methods (Joseph et al., 1976), designated δ-1 here, adopt a HG phase function whereby the scaling factor $f = g_1^2$ is used to calculate $g^* = (g_1 - f)/(1 - f)$ and $\tau^*_{sca} = (1 - f)\, \tau_{sca}$. RRTMG uses the first term in the Mie expansion for liquid-water clouds and hence δ-1 scaling. Another approach, designated δ-2, uses the Mie phase function's second term, $f = g_2$, and the revised g^* and τ^*_{sca} are calculated as for δ-1. This isotropic-equivalent method, designated δ-0, drops the asymmetry factor in the phase function and calculates a reduced τ^*_{sca} using $f = g_1$ and

the above formulae. An example of the δ-methods is listed in **Table 2**. δ-0 is the least forward scattering with the largest reduction in τ_{sca} (1–f = 0.14); δ-2 has the next largest reduction (1–f = 0.20); while δ-1 has the least (1–f = 0.25), reducing τ_{sca} by only a factor of 4. SJ versions have been coded that rewrite the cloud optical depth and scattering phase function in accord with δ scaling and are designate eponymously as *SJ/δ0, SJ/δ1,* and *SJ/δ2*.

Rayleigh scattering by gases ($P_{Ray} = 1 + ½ P_2$) can only be treated as isotropic in two-stream solutions. We evaluate this error with a version *SJ/Ray* in which the Rayleigh scattering phase function is changed to isotropic and find that the errors are as expected (viz., isotropic scattering, without the backscatter lobe of the $\cos^2(\Theta)$ term, has less reflected light), but are trivially small (~0.01 W m^{-2}, see ***T1/R5***).

The HG and δ-scaling tests here are run without ice clouds to aid in comparisons with RRTMG (see below). Global mean HG errors are [–0.05, 0.14, –0.09 W m^{-2}] for the 3 primary components (see ***T1/R8***). This pattern--less reflection and less forward scattered to the surface--is caused by the weaker forward and backward scattering peaks in the HG phase function. Although these mean errors are modest, there is no basis and no cost advantage to using 8-term HG phase functions.

Solar-J does not have a 2-stream option and thus δ-scaling calculations use a truncated phase function with full 8-stream scattering (***T1/R9-10-11***). The δ-scaling errors are modest in terms of global mean, within ±0.4 W m^{-2} for any of the three primary components (***T1/R9-10-11***). The pattern is interesting in that all three methods show a similar –0.3 W m^{-2} error in reflected flux, but the surface absorption error shifts from +0.07 to +0.23 to +0.44 W m^{-2} in the order δ-1 to δ-2 to δ-0, being caused by the increasing scaling of τ_{sca}. Thus in δ-1 the reduction in reflected flux goes into atmospheric heating; while in δ-2 and δ-0, it goes into surface heating.

These small errors in the global mean are deceiving. The δ-scaling 2-stream models are optimized to give reasonable averages, being accurate at one SZA between 0° and 90°, but having large opposite-sign errors at others (Joseph et al., 1976; Wiscombe, 1977). Examining the geographic pattern of δ-scaling errors for fixed sun (00Z) in **Figure 3**, we see that SZA ~ 40° (green dashed oval) is the zero-error point for all three δ-scaling methods. The 3 columns (a-b-c) in **Figure 3** show the 3 primary components: reflected flux, atmospheric absorption, and surface absorption, respectively. The first 3 rows (i-ii-iii) show the sequence δ-0 to δ-2 to δ-1, respectively, in order of decreasing scaling factors. Looking at the region with SZA < 40° (inside the green oval), we see that the error in reflected flux is positive and greatest for δ-0 and decreases along the sequence. Outside this oval, the error is negative, becoming less negative along the same sequence. For surface absorption, the error in δ-scaling is opposite in sign (negative inside SZA < 40 and positive outside) and follows the same δ-scaling. For atmospheric absorption, the error sequence inside the oval goes from overall negative, to small positive, to strongly positive. Because the error is consistent for SZA > 40°, when we average over the day the higher latitudes (50°S-70°S and 30°N-50°N) have consistent errors, ~2 W m^{-2}. In terms of reflection and surface absorption, δ-1 scaling has consistently smaller errors than δ-0 or δ-2.

Tropospheric heating rate profiles (W m^{-2} hPa^{-1}) for high sun (SZA > 40° at 00Z) and liquid water clouds are shown in **Figure S1a** for *SJ* (standard Mie), *SJ/HG*, and *RRTMG* (standard δ-1

scaling). The 3 profiles show the peak heating due to low (1 km) and mid-level (5 km) clouds and differ by less than 5% except near the surface. The errors relative to *SJ* are shown in **Figure S1b** along with profiles of the 3 δ-scaling errors. It is interesting that *SJ/HG* and *SJ/δ1* have similar error profiles that are quite different from those of *SJ/δ0* and *SJ/δ2*. *RRTMG* shows reduced heating in the cloudy levels with compensating increase in the clear levels. The larger *RRTMG* error near the surface (10%) may be caused by different treatments of the lower boundary in the scattering codes.

To estimate the errors in 2-stream vs. 8-stream scattering, we compare *RRTMG* with *SJ/δ1* (***T1/R12***). Including only liquid water and averaged clouds we can ensure that both models use the same optical properties (i.e., optical depth, single scattering albedo, asymmetry parameter g_1). In terms of the 3 primary components, the error is large, [–1.1, –0.8, +1.9 W m^{-2}]. The geographic pattern of this difference, shown in **Figure 3(iv)**, is uniform across SZA and quite different from the δ-scaling errors. There is a clear-sky bias between *RRTMG* and *SJ* (***T1/R4***) that is in the opposite sense and combining these two differences leads to an estimated 2-stream versus 8-stream error of [–2.4, –0.4, +2.7 W m^{-2}] (***T1R13***), which may be slightly exaggerated because the clear-sky bias is not additive and would not apply to the regions with liquid clouds. This comparison is not ideal because there may be unknown differences in the scattering models of the two codes. Nevertheless, 2-stream scattering appears to produce excess surface absorption of at least 2 W m^{-2}.

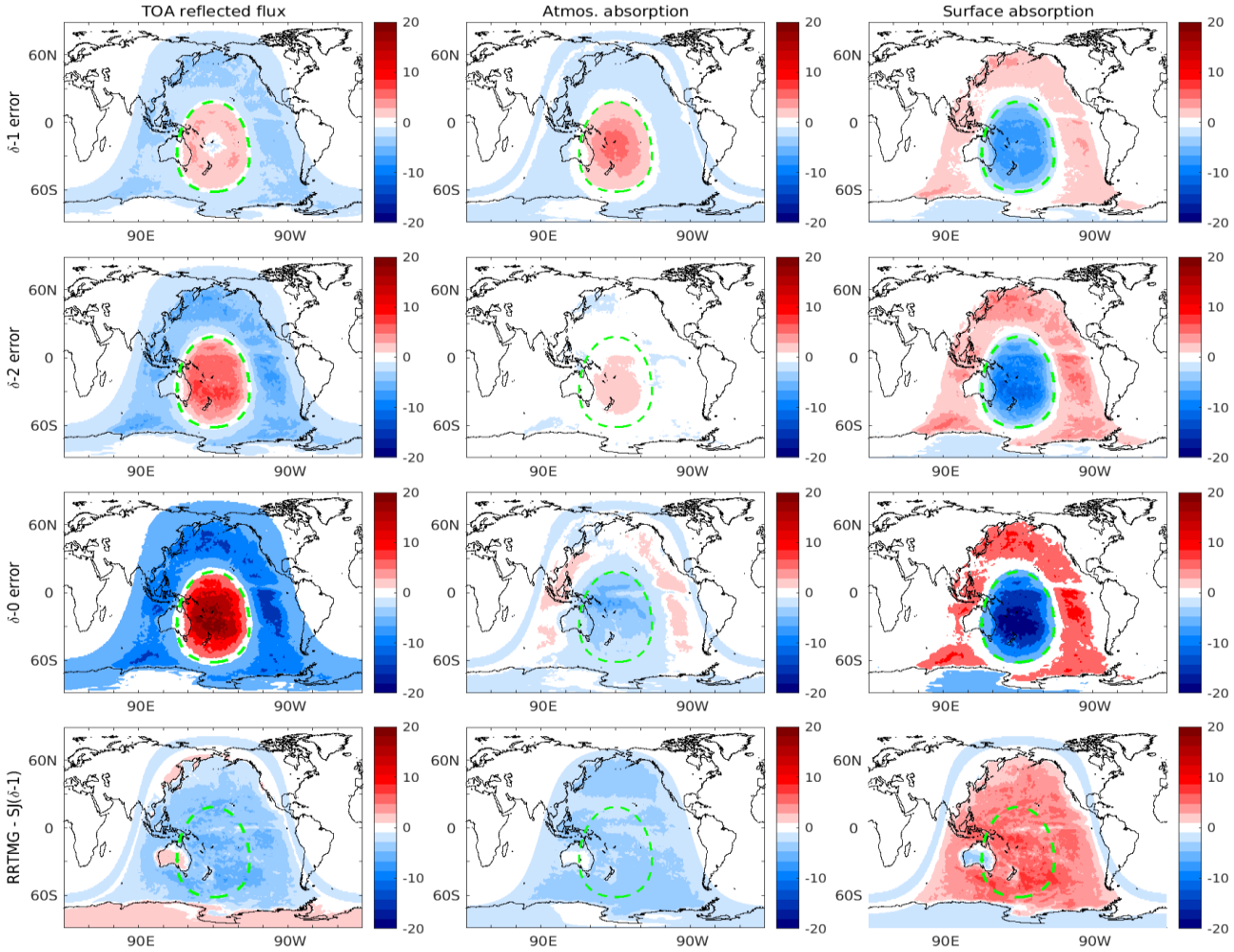

Figure 3. Geographic map of model differences in solar heating terms (W m^{-2}) averaged over 31 days in January at 00Z (sun over the Dateline), including only liquid water and averaged clouds (i.e., fractional clouds spread over the grid cell). The green dashed line encloses the region with SZA < 40°. Columns show **(a)** reflected flux, **(b)** atmospheric absorption and **(c)** surface absorption. Rows **(i)**, **(ii)** and **(iii)** show errors for δ-1, δ-2 and δ-0, respectively, calculated with Solar-J 8-stream scattering relative to the standard Mie phase function, see Table 2. Row **(iv)** shows the differences RRTMG-SW (default δ-1 scaling) minus Solar-J (δ-1 scaling).

295

4. Ice-cloud optics

Ice particles in cirrus or mixed-phase clouds come in a wide range of sizes and shapes (Kaercher et al., 2014) with a dizzying array of optical properties (Mishchenko et al., 2016; Yang et al., 2018). Solar heating codes adopt a simplified parameterization. RRTMG primarily uses a Fu (1996) parameterization for optical depth, single scattering albedo, and asymmetry parameter. Solar-J adopts an effective radius based on ice water concentration (Heymsfield et al., 2003), the full scattering phase functions for two typical mixes of particle shape (cold and colder, Mishchenko et al. (1996), and the observed refractive index of ice water.

We compare *RRTMG* and *SJ* using averaged clouds (no overlap model needed). Without ice water clouds, the two models produce similar tropospheric heating rates (**Figure 4a**). Both models use the same optical properties for liquid water clouds, and thus difference here (±0.05 K per day) reflect the treatment of scattering (i.e., 2-stream δ-1scaling vs. 8-stream Mie phase function). With ice water clouds included, however, the two models clearly diverge (**Figure 4b**): *RRTMG* heating rates are 0.1 to 0.2 K per day less than those in *SJ* throughout the middle-upper troposphere, with the pattern reversed for liquid water clouds in the tropics (2 – 6 km). These differences are a large fraction (10-20%) of the total heating rate. If we run the models with full clouds using MAX-RAN cloud overlap, the results are similar (**Figure 4c**), see Section 5 below for discussion on cloud overlap.

The treatment of ice-water clouds is clearly a large source of error in solar-heating codes. We believe that the Solar-J approach is more physically based and probably more accurate than RRTMG, but both codes are likely in error, with the model differences here providing a lower estimate of the error. A more accurate treatment of ice water clouds will combine the physics of individual particles (e.g., Yang et al. 2018; Mishchenko et al 2016) with the actual mix of such particles observed in the atmosphere (Heymsfield et al., 2017; Thornberry et al., 2017).

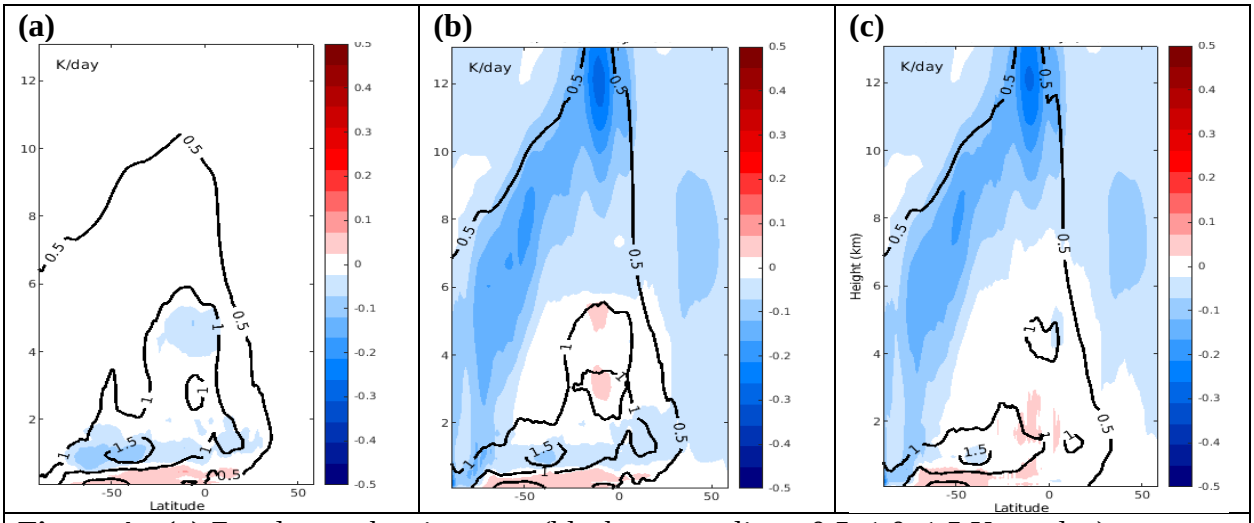

Figure 4. **(a)** Zonal mean heating rates (black contour lines, 0.5, 1.0, 1.5 K per day) as a function of latitude and height for January 2015 using Solar-J with averaged clouds and no ice water clouds. Color fill (-0.5 to +0.5 K per day color bar, with ±0.025 as white) show the difference RRTMG-SW v4.0 minus Solar-J. **(b)** Same as (a) except that ice water clouds are

included. **(c)** Same as (b) except that MAX-RAN cloud overlap is used to generate ICAs; and RRTMG uses McICA to sample the ICAs, while Solar-J uses QCAs (see text).

5. Cloud overlap

When grid-cell layers specify fractional cloud cover (presumably in terms of areal coverage), explicit information or an algorithm is needed to describe exactly how they overlap. A typical algorithm is MAX-RAN (Briegleb, 1992): when two adjacent vertical layers have clouds, they are maximally overlapped; but when two cloudy layers, or two groups of maximally overlapped clouds, are separated by a clear layer, they are randomly overlapped (e.g., see figures in Neu et al., 2007). More realistic cloud-overlap algorithms have been developed based on observations showing that cloud overlap has a vertical decorrelation length (Barker, 2008; Di Giuseppe & Tompkins, 2015; Tompkins & Di Giuseppe, 2015). The EXP-RAN method assumes an exponential decorrelation length for connected cloud layers but random overlap across clear layers (Tompkins & Di Giuseppe, 2007). Solar-J uses the MAX-COR approach developed in Cloud-J (Prather, 2015) that was designed to (i) be linear in cost with increasing numbers of layers and (ii) more robust when cloud data are averaged in time or space, which tends to eliminate cloud-free layers. Based on observations of decorrelation length (Kato et al., 2010; Naud et al., 2008; Oreopoulos et al., 2012; Pincus et al., 2005), MAX-COR defines 6-layer groupings by altitude range with MAX overlap within each group and with partial, not random, overlap of each MAX group with its neighbor. The *RRTMG* code assumes MAX-RAN cloud overlap as do most models. Within Solar-J we can run both MAX-RAN (*SJ/RAN*) and the standard MAX-COR (*SJ*) to calculate the difference caused by these assumptions (see discussion below)**.**

Cloud overlap algorithms generate a set of Independent Column Atmospheres (ICAs) to fill each grid cell. Each ICA has a fractional area, and each layer in the ICA is fully clear or cloudy. A major assumption is that ICAs are independent (i.e., neighbor-neighbor relationships are not defined) and thus can be solved with 1D RT as horizontally homogeneous, plane parallel layers. New approaches to include neighboring clouds (i.e., in an adjacent ICA) are being developed (Hogan & Bozzo, 2018). Ideally, one would solve each ICA and then average the solar heating, but the number of ICAs makes this task difficult: e.g., in a moderate resolution atmosphere (0.5 degree cells and 60 layers) the average number of ICAs is ~20 and the maximum number can exceed 100 (see Figure 2 in Prather, 2015).

Given a set of ICAs for a grid cell, we have two practical methods for approximating the average solar heating. RRTMG randomly selects an ICA for each wavelength bin in the RT solution, a method designated Monte Carlo ICA (McICA, Pincus et al., 2003). McICA clearly has large errors in each time step with global mean rms errors reaching 40 W m^{-2} (Pincus et al., 2003; Barker et al., 2008). A key underlying assumption is that solar heating errors propagate symmetrically and linearly in the climate system. Assessing net errors caused by noisy heating rates would need to examine hydrology, cloud systems, primary productivity and air quality in Earth system models. Solar-J selects up to 4 representative quadrature column atmospheres (QCAs) with fractional areas to represent the distribution of ICAs and does full wavelength integrations for each QCA (Neu et al., 2007). See **Figure S2** for the average fractional area of

the 4 QCAs. Cloud quadrature does a very good job of averaging over the ICAs with net bias errors of ~1% in solar intensity and rms errors of 2-4%. To reach equivalent accuracy for a single time step using random selection would require about 50 ICAs versus an average of 2.8 QCAs. (Many grid cells use less than 4 QCAs.)

The cloud overlap assumption is an important source of error. Comparing MAX-RAN (*SJ/RAN*) minus MAX-COR (*SJ*) within a consistent Solar-J framework (***T1/R14***) shows that differences in the 3 primary components are moderate and fairly uniform, [-1.4, -0.1, +1.4 W m^{-2}], shifting 1.4 W m^{-2} from reflection to surface absorption. The forced decorrelation of deep vertically continuous cloud layers with MAX-COR leads to a slightly greater overall cloud fraction in most cases and more cloud-scattered reflected sunlight with parallel reduction in surface heating. Atmospheric absorption is much less affected because the total water path and optical properties averaged over the QCAs are identical in either model.

Solar-J cannot do a McICA calculation and thus we must compare *RRTMG* (MAX-RAN overlap, McICA, and δ-1 scaling) with *SJ/RAN* (MAX-RAN, QCA, and 8-term Mie phase function). We do this comparison not just with water clouds because the ice clouds are an important component in generating the MAX-RAN ICAs. As found above, there are notable differences between RRTMG and Solar-J due to δ-1 scaling, 2-stream scattering, and treatment of ice clouds. As first order estimate of the differences not involving ICA methods, we calculate *RRTMG* minus *SJ* using averaged clouds (***T1R15***) and find a primary component difference of [-0.4, -2.7, +3.0 W m^{-2}]. Next, we calculate *RRTMG* minus *SJ/RAN* (both using MAX-RAN overlap) and find a difference of [-2.1, -2.4, +4.4 W m^{-2}] (***T1/R16***). Subtracting these, we infer a McICA minus QCA difference of [-1.7, +0.3, +1.4 W m^{-2}]. The inference assumes that these changes are additive. Surprisingly, this bias is not close to zero. Ice water clouds do not appear to be responsible because the differences in atmospheric heating for average cloud (**Figure 4b**) and MAX-RAN overlap (**Figure 4c**) are similar in the ice cloud regions, but differ in the liquid cloud region. Possibly, the McICA minus QCA difference shows up here because with MAX-RAN we have some ICAs with very thick liquid clouds, for which δ-1 and 2-stream errors are much greater than they are in the averaged-cloud case or in ice clouds, which are thin in either case. Possibly, the MAX-RAN generation of ICAs is slightly different in each code. Whatever the cause, we believe that this double difference is not a good measure of the difference between McICA and QCA, because there are some biases between RRTMG and Solar-J that occur under different cloud conditions. We must seek a different set of code configurations to evaluate McICA-QCA error.

As shown by the McICA developers, large rms errors occur with this Monte Carlo approach. Unlike Solar-J QCAs, the RRTMG McICA approach guarantees the hourly total water path and effective optical properties used are not the average of the ICAs upon which they are based. For example, the wavelength bins with large cloud absorption may pick an ICA with minimal water path. While this averages out over a great enough number of calls, large hourly local rms errors in atmospheric heating rates may be more important than the mean difference, as it is occurring over the lifetime of individual clouds.

6. Ocean surface albedo

Most solar heating modules assume that the ocean surface albedo (OSA) is constant, typically 0.06 as used in the ECMWF data here, for all incident solar direct and diffuse radiation. OSA varies greatly with incident angle and somewhat with wavelength, wind speed, and chlorophyll concentrations (Jin et al., 2004; Jin et al., 2011; Li et al., 2006). See **Figure S3**. Recently, this interactive parameterization of OSA (Jin et al., 2011) has been implemented in two French Earth system models (Seferian et al., 2018) and shown to much better match satellite derived OSA. Here we take the FORTRAN module directly from Séférian with only minor modifications. Because Solar-J resolves the downward diffuse radiation with 4 angles, we calculate the albedo specifically for those angles plus the direct solar beam, and do not use the OSA parameterization for diffuse radiation.

Solar-J lower boundary condition is 2nd-order in finite-difference RT solution and has not changed since the original Fast-J documentation (Wild et al., 2000). Unfortunately, the interactive OSA requirement that each angle has a different albedo required a substantial revision. The Fast-J Feautrier solver for scattered light (see equations 9 & 19 of Wild et al., 2000) uses odd-even (leap-frog) first-order finite-difference equations, solving at the lower boundary for j_n.

$$j_n = ½ [I^{up}(+u_n) + I^{down}(-u_n)] \equiv ½ [I^{up}{}_n + I^{down}{}_n], \quad (1)$$

where u_n (n=1:4) are the cosines of the zenith angles for the scattered intensity (I). The angles are Gauss points with weights w_n. We assume a Lambertian reflective surface, and hence $I^{up}(+u_n)$) is isotropic and denoted simply as I^{up}. The solution requires a linear equation relating I^{up} to the intensities at the 4 angles $j_{n=1:4}$. For notation below, we use Σ to denote the sum over the quadrature angles n = 1:4. The upward flux from the lower boundary is the cosine-weighted sum of the specific intensity

$$F^{up} = 2 \Sigma I^{up} u_n w_n = I^{up}, \text{ where } \Sigma u_n w_n \equiv ½ \quad (2)$$

The upward flux can also be calculated in terms of the downward incident fluxes at the 4 quadrature angles and direct beam, but with angle-specific albedos A_n and A_0.

$$F^{up} = 2 \Sigma A_n I^{down}{}_n u_n w_n + ¼ A_0 u_0 F^{solar} \quad (3)$$

Substituting $I^{down}{}_n = 2 j_n - I^{up}$ from equation (1), we get

$$I^{up} = F^{up} = 2 \Sigma A_n (2 j_n - I^{up}) u_n w_n + ¼ A_0 u_0 F^{solar}$$
$$= 4 \Sigma j_n A_n u_n w_n - 2 I^{up} \Sigma A_n u_n w_n + ¼ A_0 u_0 F^{solar} \quad (4)$$

If A is a constant, this reduces to equation 19 of Wild et al. (2000).

$$I^{up} = [4A / (1+A)] \Sigma j_n u_n w_n + [A / (1+A)] A_0 u_0 F^{solar} \quad (5)$$

With A_n depending on u_n, we derive the new lower boundary condition for I^{up}.

$$I^{up} = [4 / (1+2 \Sigma A_n u_n w_n)] [\Sigma j_n A_n u_n w_n + ¼ A_0 u_0 F^{solar}] \quad (6)$$

Evaluation of interactive OSA (*SJ* minus *SJ/OSA*) uses the full spherical geometric atmosphere with MAX-COR cloud overlap. The global mean errors with fixed OSA are [+0.7, +0.2, -0.8 W m^{-2}] for [reflection, atmospheric absorption, and surface absorption], respectively (***T1/R17***). The global mean error, fixed minus interactive, can be adjusted to near zero by selecting the fixed OSA, but there remains a strong latitudinal error of 3 W m^{-2} in ocean heating associated with high sun, see **Figure 5**. The zonal rms errors are large, 2 to 8 W m^{-2}, because of the wide diurnal range of solar zenith angles over the day, but given the thermal inertia of the upper ocean layers, this probably averages out. Overall, these results are similar to those found in Séférian et al. (2018).

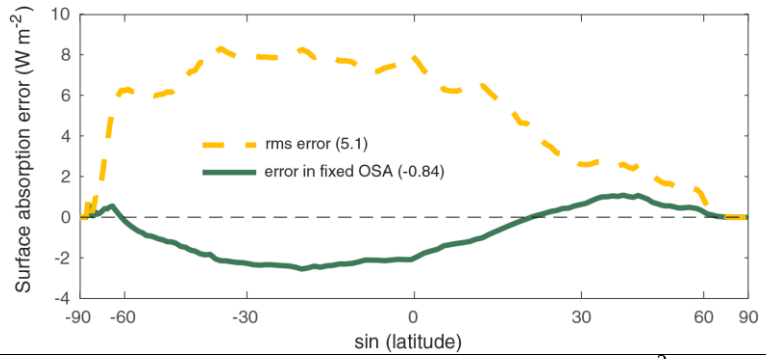

Figure 5. Zonal mean error (mean and rms in W m^{-2}) for fixed ocean surface albedo (OSA) versus interactive OSA that depends on wavelength, incident angle and wind.

7. Findings and recommendations

The findings from this work and the previous one on spherical atmospheres (P2019) identify a range of errors in current solar heating codes used in climate and Earth system models. Here, we make recommendations based on the magnitude of error and the difficulty or extra computational cost in improving the models. The levels of ranking include 0 (inconsequential errors), 1 (modest errors and easy/cost-effective fix, or significant errors but hard to fix), 2 (significant errors and easy/cost-effective fix).

a) ***Spherical, refracting atmosphere, level 2***. The errors caused by flat-atmosphere models are on the order of 1-2 W m^{-2} and much larger in twilight regions. Spherical solar ray-tracing with refraction can and should be readily implemented with simple ray tracing code (P2019) and incorporated in standard 2-stream codes (Spurr and Natraj, 2011). There will be minor costs in that about 56% of the Earth, rather than 50%, will require radiation calls every time step.

b) ***Geometrical, expanding atmosphere, level 1.*** Shifting from geopotential to geometric coordinates is a conceptual change and will need more thought on how to account for the extra mass in the upper layers as well as the extra solar heating.

c) ***Stratospheric heating, level 1***. Errors in stratospheric heating rates for codes like RRTM-SW are caused by the inadequate resolution of O_3 and O_2 absorption and are significant (~10%, see Figure 2 of H2017). These can and should be readily corrected by adding 2-4 bins in the ultraviolet (2-4% overall cost increase).

d) ***UV-visible spectrum binning, level 1***. The 300-778 nm sunlight that reaches the surface interacts primarily with broad band features of O_3 absorption (Hartley-Huggins and Chappuis bands) and Rayleigh scattering. The disturbing differences, ~1 W m^{-2}, between RRTM (4 super-bins) and Solar-J (7 super-bins) in this apparently simple region indicate that an off-line study with super-resolved set of bins (~0.1 nm) could easily establish an optimal set of super-bins.

e) ***Resolving cloud absorption, level 2.*** The super-bins (#19 through #27 in RRTM) need to be reformulated to more accurately account for the absorption spectrum of liquid and ice water. The error is great in terms of atmospheric absorption (current super-bins have on

494 average ~2 W m^{-2} excess heating) and cloud-top heating (25% too great). Unfortunately,
495 this is a major research task, requiring new calculation of the sub-bins. It is not clear if
496 the new spectral model would invoke extra computational cost (more total sub-bins).
497 f) ***Rayleigh scattering, level 0.*** Forcing Rayleigh scattering to be isotropic, as required in
498 current 2-stream codes, is inconsequential.
499 g) ***Multi-stream scattering, level 1***. The errors caused by δ-1 scaling of all scattering phase
500 functions is tied to the error caused by 2-stream scattering codes. It is difficult to
501 quantify here, but together leads to moderately large systematic errors: about 2 Wm^{-2} less
502 reflected flux and more surface heating. The solution requires multi-stream scattering
503 codes like Solar-J, for which no scaling of the phase function for clouds and aerosols is
504 necessary. The problem is that multi-stream scattering is clearly more computationally
505 expensive and possibly difficult for long-term climate simulations. A benchmark multi-
506 stream solar heating code with no phase function scaling could be used for decade
507 climate simulations in atmosphere-only mode.
508 h) ***Ice clouds, level 2.*** The errors caused by current ice-cloud parameterizations are very
509 worrisome, 0.1 to 0.2 K per day on average for much of the upper troposphere. They
510 could not be quantified here because both models have weak parameterizations. A more
511 accurate treatment of ice water clouds is needed, combining the physics of individual
512 particles with the actual mix of such particles in the atmosphere. This is a research task,
513 but the implementation of better ice-cloud physics will not increase computational costs
514 unless it is accompanied by multi-stream scattering (g).
515 i) ***Cloud overlap, level 2.*** The two different cloud overlap algorithms tested here, MAX-
516 RAN vs. MAX-COR, make a difference of about 3 W m^{-2} in reflected versus surface
517 absorption. MAX-COR is meant to be an improvement over MAX-RAN, but there are
518 other overlap options (e.g., EXP-RAN, Tompkins & Giuseppe, 2007) that probably show
519 similar differences. It is important to establish some standard, community-wide, satellite-
520 based cloud overlap models (Barker, 2008; Kato et al., 2010; Ham et al., 2015; Bankert et
521 al., 2015; Tompkins and Giuseppe, 2015) along with a simple ICA generator (e.g.,
522 Prather, 2015) that the community could easily implement in solar heating codes and test
523 in climate models.
524 j) ***ICA averaging, level 1***. Using cloud quadrature QCAs to average over ICAs would
525 greatly reduce the large numerical rms noise generated by McICA. It is easy to
526 implement in any code, but would increase the computational costs by a factor of 2.8.
527 k) ***Ocean surface albedo, level 2***. Use of an interactive ocean surface albedo that depends
528 on SZA, wind and wavelength would eliminate a latitudinal mean bias of 3 W m^{-2} in
529 surface absorption. This easy fix and has already been implemented in the ARPEGE and
530 LMDZ models (Séférian, R. et al., 2017).
531 l) ***Photosynthetically Active Radiation, no assessment.*** PAR is calculated directly in
532 Solar-J with 4 downward diffuse streams and no δ-scaling of cloud optical depth, which
533 is notably more accurate than 2-stream codes, see (g) above. We estimate that PAR
534 errors are level 2, but a more thorough analysis would need to couple the direct and
535 diffuse PAR to a land biosphere model to evaluate the errors in primary productivity.
536
537 **Data Availability Statement**
538

Dataset, Solar-J source code, and scripts for generating figures and tables are concurrently submitted to DRYAD University of California, Irvine with DOI https://doi.org/10.7280/D1PQ3W.

Acknowledgements. This work was developed with support from the US Department of Energy, Office of Science, Biological and Environmental Research Program (award DE-SC0012536); Lawrence Livermore National Laboratory (subcontract B628407) under the E3SM project; and the NASA Modeling, Analysis and Prediction program (award NNX13AL12G).

548

Table 1. Errors in the three primary components of the solar radiation budget (reflected sunlight, atmospheric absorption, surface absorption in W m^{-2}) for a range of approximations in the radiative transfer models.

row	models	error being estimated	mean difference (W m^{-2})			rms difference (W m^{-2})		
			refl.	atm.	surf.	refl.	atm.	surf.
Wavelength binning errors for near IR gas absorption with clear sky								
1	B1 – B0	CLIRAD gas absorption >700nm	+0.94	-5.68	+4.73	1.4	8.4	7.0
2	B2 – B0	LLNL gas absorption > 700 nm	+0.53	-7.66	+7.13	1.2	12.0	11.0
3	B3 – B0	RRTM v. RRTMG gas absorption >700 nm	+0.03	-0.24	+0.21	0.0	0.4	0.3
4	R0 − B0	AER's v4.0 RRTMG v. SJ/RRTMG	+1.30	-0.47	-0.82	1.9	0.8	1.4
5	MR –B0	isotropic Rayleigh scattering	-0.01	+0.01	0.00	0.0	0.1	0.0
Wavelength binning errors for clouds *(MAX-COR overlap and QCAs, no IR gas absorption*)								
6	C1 – C0	CLIRAD cloud absorption bins	-2.14	+3.85	-1.70	8.7	10.4	3.1
7	C2 – C0	RRTM cloud absorption bins	-1.14	+1.68	-0.51	2.2	3.2	1.1
Scattering phase function errors for HG and δ-scaling using grid-cell averaged liquid water clouds. Also differences between RRTMG-SW v4.0 and *Solar-J* using δ-1 scaling. The sum of the 3 principal components may not equal zero because of round-off or small differences in incident flux (not shown) due to the vertical gridding of clouds in *SJ*.								
8	Mh–M0	HG v. Mie (liq cld)	-0.05	0.14	-0.09	0.8	0.6	0.6
9	M1–M0	δ-0 v. Mie (liq cld)	-0.26	-0.22	+0.44	5.6	1.2	5.1
10	M2–M0	δ-1 v. Mie (liq cld)	-0.33	+0.23	+0.07	1.4	1.0	2.2
11	M3–M0	δ-2 v. Mie (liq cld)	-0.32	+0.05	+0.23	2.8	0.5	3.1
12	R2– M2	RRTMG v. SJ δ-1 (liq cld)	-1.14	-0.82	+1.88	3.0	1.7	4.1
13	Row 12 - Row 4	2-stream v. 8-stream (estimated)	-2.44	-0.35	+2.70	-	-	-
Cloud Overlap Algorithm. *Solar-J* with QCAs for both MAX-RAN and MAX-COR overlap. RRTMG-SW v4.0 run with McICA for MAX-RAN cloud overlap. See note above small differences in incident flux.								
14	D1 − D0	SJ (MAX-RAN) v. SJ (MAX-COR) both QCA	-1.35	-0.06	+1.41	7.9	1.0	8.6
15	R1– M4	RRTMG (avg cld) v. SJ (avg cld)	-0.38	-2.67	+2.97	4.4	5.9	6.1
16	R3 − D1	RRTMG (McICA) v. SJ (QCA) both MAX-RAN	-2.10	-2.36	+4.41	18.5	5.9	20.5

Ocean Surface Albedo *(Solar-J with MAX-COR overlap and QCAs)*								
17	O1− O0	fixed OSA v. varying OSA	+0.68	+0.16	-0.84	4.7	0.4	5.1
Notes: See methods section **Table S1-2** for description of each of the pairs of simulations noted in column two. Global-mean area-weighted differences are averaged over January 2015 (744 hourly data) with root mean square differences accumulated hourly. All results use the UCI CTM and the T159L60 (~1.1º x 1.1º) ECMWF forecast fields developed by U. Oslo from the Open-IFS system (Søvde et al., 2012; Prather et al., 2017).								

549
550

Table 2. Parameters (scaling factor *f*, asymmetry factor g^*, scattering optical depth τ^*_{sca}) for different delta-M scaling methods. This example assumes liquid water cloud (R_{eff} = 12 μm, wavelength = 600 nm, ω_0 = 0.99999). The Mie phase function is truncated after P_7. The Henyey-Greenstein phase function is expanded to P_7 is using only the first asymmetry term of the Mie phase function. The δ-0, δ-1 and δ-2 phase functions include at most P_0 and P_1.

$P_{Mie}(\Theta) = 1 + 0.865 \times 3P_1(\cos(\Theta)) + 0.795 \times 5P_2(\cos(\Theta)) + \ldots + 0.507 \times 15P_7(\cos(\Theta))$

$P_{HG}(\Theta) = 1 + 0.865 \times 3P_1(\cos(\Theta)) + 0.748 \times 5P_2(\cos(\Theta)) + \ldots + 0.362 \times 15P_7(\cos(\Theta))$

Method	*f*	$g^* = (g_1 - f)/(-f)$	$\tau^*_{sca}/\tau_{sca} = (1-f)$	notes
δ-0 (isotropic)	$g_1 = 0.865$	0	*0.135*	$g_n=0, n\geq 1$
δ-1	$g_1^2 = 0.748$	*0.464*	*0.253*	$g_n=0, n\geq 2$
δ-2	$g_2 = 0.795$	*0.342*	*0.205*	$g_n=0, n\geq 2$

551
552

References

Bankert, R.L., and J.E. SolBrig (2015*).* Cluster Analysis of A-Train Data: Approximating the Vertical Cloud Structure of Oceanic Cloud Regimes*. Journal Applied Meteorology and Climatology,* 54: 996-1008, doi.org:10.1175/JAMC-D-14-0227.1

Barker, H. W. (2008). Representing cloud overlap with an effective decorrelation length: An assessment using CloudSatand CALIPSO data*. Journal of Geophysical Research-Atmospheres.*,113, D24205, doi:10.1029/2008JD010391.

Bian, H. S., & Prather, M. J. (2002). Fast-J2: Accurate simulation of stratospheric photolysis in global chemical models*. Journal of Atmospheric Chemistry,* 41(3), 281-296.

Boucher, O. (1998). On aerosol direct shortwave forcing and the Henyey-Greenstein phase function. *Journal of the Atmospheric Sciences*, 55(1), 128-134.

Briegleb, B. P. *(*1992). Delta-Eddington Approximation for Solar-Radiation in the Ncar Community Climate Model. *Journal of Geophysical Research-Atmospheres,* 97(D7), 7603-7612.

Chou, M.D. (1992). A solar-radiation model for use in climate studies. *Journal of Atmospheric Sciences* 49, 762-772.

Chou, M. D., & Suarez, M. (1996). A solar radiation parameterization (CLIRAD-SW). *NASA Tech. Memo*. 104606, 15, 48 pp.

Clough, S. A., Shephard, M. W., Mlawer, E., Delamere, J. S., Iacono, M., Cady-Pereira, K., et al. (2005). Atmospheric radiative transfer modeling: a summary of the AER codes. *Journal of Quantitative Spectroscopy and Radiative Transfer*, 91(2), 233-244.

Di Giuseppe, F., & Tompkins, A. M. (2015). Generalizing Cloud Overlap Treatment to Include the Effect of Wind Shear*. Journal of the Atmospheric Sciences, 72(8), 2865-2876.*

Etminan, M., Myhre, G., Highwood, E. J., & Shine, K. P. (2016). Radiative forcing of carbon dioxide, methane, and nitrous oxide: A significant revision of the methane radiative forcing. *Geophysical Research Letters,* 43(24), 12614-12623.

Fang, T. M., Wofsy, S. C., & Dalgarno, A. (1974). Opacity Distribution Functions and Absorption in Schumann-Runge Bands of Molecular-Oxygen. *Planetary and Space Science*, 22(3), 413-425.

Fu, Q. (1996). An Accurate Parameterization of the Solar Radiative Properties of Cirrus Clouds for Climate Models, *Journal of Climate*, 9, 2058–2082.

Grant, K. E., & Grossman, A. S. (1998). Description of a Solar Radiative Transfer Model for Use in LLNL. *Climate and Atmospheric Chemistry Studies.* UCRL-ID(129949), 17 pp.

Ham, S.-H., S. Kato, H. W. Barker, F. G. Rose, & S. Sun-Mack (2015). Improving the modelling of short-wave radiation through the use of a 3D scene construction algorithm. *Quarterly Journal of the Royal Meteorological Society*, 141: 1870–1883, doi:10.1002/qj.2491.

Heymsfield, A. J., & Coauthors (2017). Cirrus clouds. Ice Formation and Evolution in Clouds and Precipitation: Measurement and Modeling Challenges. *Meteorological Monographs.*, doi:https://doi.org/10.1175/AMSMONOGRAPHS-D-16-0010.1.

Heymsfield, A. J., Matrosov, S., & Baum, B. (2003). Ice water path-optical depth relationships for cirrus and deep stratiform ice cloud layers. *Journal of Applied Meteorology*, 42, 1369-1390.

Hogan, R. J., & Bozzo, A. (2018). A Flexible and Efficient Radiation Scheme for the ECMWF Model. *Journal of Advances in Modeling Earth Systems*, 10(8), 1990-2008.

Hsu, J., Prather, M. J., Cameron-Smith, P., Veidenbaum, A., & Nicolau, A. (2017). A radiative transfer module for calculating photolysis rates and solar heating in climate models: Solar-J v7.5. *Geoscientific Model Development*, 10(7), 2525-2545.

Jin, Z. H., Charlock, T. P., Smith, W. L., & Rutledge, K. (2004). A parameterization of ocean surface albedo. *Geophysical Research Letters*, 31(22).

Jin, Z. H., Qiao, Y. L., Wang, Y. J., Fang, Y. H., & Yi, W. N. (2011). A new parameterization of spectral and broadband ocean surface albedo. *Optics Express*, 19(27), 26429-26443.

Joseph, J. H., Wiscombe, W. J., & Weinman, J. A. (1976). Delta-Eddington Approximation for Radiative Flux-Transfer. *Journal of the Atmospheric Sciences*, 33(12), 2452-2459.

Kärcher, B. Dörnbrack A, Sölch I. (2014). Supersaturation variability and cirrus ice crystal size distributions. *Journal of Atmospheric Sciences,* 71: 2905 – 2926.

Kato, S., S. Sun-Mack, W. F. Miller, F. G. Rose, Y. Chen, P. Minnis, & B. A. Wielicki (2010). Relationships among cloud occurrence frequency, overlap, and effective thickness derived from CALIPSO and CloudSat merged cloud vertical profiles. *Journal of Geophysical Research-Atmospheres*., 115 D00H28, doi:10.1029/2009JD012277.

Lacis, A. A., & Oinas, V. (1991). A Description of the Correlated Kappa-Distribution Method for Modeling Nongray Gaseous Absorption, Thermal Emission, and Multiple-Scattering in Vertically Inhomogeneous Atmospheres. *Journal of Geophysical Research-Atmospheres*, 96(D5), 9027-9063

Li, J., & Ramaswamy, V. (1996). Four-stream spherical harmonic expansion approximation for solar radiative transfer. *Journal of the Atmospheric Sciences*, 53(8), 1174-1186.

Li, J., Scinocca, J., Lazare, M., McFarlane, N., von Salzen, K., & Solheim, L. (2006). Ocean surface albedo and its impact on radiation balance in climate models. *Journal of Climate*, 19(24), 6314-6333.

Lin, Z. Y., Chen, N., Fan, Y. Z., Li, W., Stamnes, K., & Stamnes, S. (2018). New Treatment of Strongly Anisotropic Scattering Phase Functions: The Delta-M plus Method. *Journal of the Atmospheric Sciences*, 75(1), 327-336.

Logan, J. A., Prather, M. J., Wofsy, S. C., & Mcelroy, M. B. (1978). Atmospheric Chemistry - Response to Human Influence. *Philosophical Transactions of the Royal Society a-Mathematical Physical and Engineering Sciences*, 290(1367), 187-234.

Mishchenko, M. I., Rossow, W. B., Macke, A., & Lacis, A. A. (1996). Sensitivity of cirrus cloud albedo, bidirectional reflectance and optical thickness retrieval accuracy to ice particle shape. *Journal of Geophysical Research-Atmospheres*. 101, 16973–16985.

Mishchenko, M. I., Zakharova, N. T., Khlebtsov, N. G., Videen, G., & Wriedt, T. (2016). Comprehensive thematic T-matrix reference database: A 2014-2015 update. *Journal of Quantitative Spectroscopy & Radiative Transfer*, 178, 276-283.

Mlawer, E. J., Payne, V. H., Moncet, J. L., Delamere, J. S., Alvarado, M. J., & Tobin, D. C. (2012). Development and recent evaluation of the MT_CKD model of continuum absorption. *Philosophical Transactions of the Royal Society a-Mathematical Physical and Engineering Sciences*, 370(1968), 2520-2556.

Mlawer, E. J., Taubman, S. J., Brown, P. D., Iacono, M. J., & Clough, S. A. (1997). Radiative transfer for inhomogeneous atmospheres: RRTM, a validated correlated-k model for the longwave. *Journal of Geophysical Research-Atmospheres*, 102(D14), 16663-16682.

Myhre, G., D. Shindell, F.-M. Bréon, W. Collins, J. Fuglestvedt, J. Huang, D. Koch, J.-Lamarque, D. Lee, B. Mendoza, T. Nakajima, A. Robock, G. Stephens, T. Takemura & H. Zhang (2013). Anthropogenic and Natural Radiative Forcing. In: Climate Change 2013: The Physical Science Basis. *Contribution of Working Group I to the Fifth Assessment Report of the Intergovernmental Panel on Climate Change [Stocker, T.F., et al., eds.]*. Cambridge University Press, Cambridge, UK.

Naud, C. M., Del Genio, A., Mace, G. G., Benson, S., Clothiaux, E. E., & Kollias, P. (2008). Impact of dynamics and atmospheric state on cloud vertical overlap. *Journal of Climate*, 21(8), 1758-1770.

Neu, J. L., Prather, M. J., & Penner, J. E. (2007). Global atmospheric chemistry: Integrating over fractional cloud cover. *Journal of Geophysical Research-Atmospheres*, 112(D11), D11306.

Olson, J., M. Prather, et al. (20 authors) (1997). Results from the IPCC photochemical model intercomparison (PhotoComp), *Journal of geophysical Research-Atmospheres*, 102, 5979-5991.

690 Oreopoulos, L., Lee, D., Sud, Y. C., & Suarez, M. J. (2012). Radiative impacts of cloud
691 heterogeneity and overlap in an atmospheric General Circulation Model. *Atmospheric Chemistry*
692 *and Physics*, 12(19), 9097-9111.
693
694 Paynter, D., & Ramaswamy, V. (2014). Investigating the impact of the shortwave water vapor
695 continuum upon climate simulations using GFDL global models. *Journal of Geophysical*
696 *Research-Atmospheres*, 119(18), 10720-10737. <Go to ISI>://000344052800007.
697
698 PhotoComp (2010). Chapter 6 in SPARC CCMVal Report on Evaluation of Chemistry-Climate
699 Models (V. Eyring, T. G. Shepherd, D. W. Waugh, eds.), *SPARC Report No. 5*, WCRP-30/2010,
700 WMO/TD – No. 40. https://www.spar-climate.org/publications/sparc-reports/.
701
702 Pincus, R., Barker, H. W., & Morcrette, J. J. (2003). A fast, flexible, approximate technique for
703 computing radiative transfer in inhomogeneous cloud fields. *Journal of Geophysical Research-*
704 *Atmospheres*, 108(D13).
705
706 Pincus, R., Hannay, C., Klein, S. A., Xu, K. M., & Hemler, R. (2005). Overlap assumptions for
707 assumed probability distribution function cloud schemes in large-scale models. *Journal of*
708 *Geophysical Research-Atmospheres*, 110(D15).
709
710 Pincus, R., Mlawer, E. J., Oreopoulos, L., Ackerman, A. S., Baek, S., Brath, M., et al. (2015).
711 Radiative flux and forcing parameterization error in aerosol-free clear skies. *Geophysical*
712 *Research Letters*, 42(13), 5485-5492.
713
714 Prather, M. J. (2015). Photolysis rates in correlated overlapping cloud fields: Cloud-J 7.3c.
715 *Geoscientific Model Development*, 8(8), 2587-2595.
716
717 Prather, M.J., Xin Zhu, Clare M. Flynn, Sarah A. Strode, Jose M. Rodriguez, Stephen D.
718 Steenrod, Junhua Liu, Jean-Francois Lamarque, Arlene M. Fiore, Larry W. Horowitz, Jingqiu
719 Mao, Lee T. Murray, Drew T. Shindell, & Steven C. Wofsy (2017). Global Atmospheric
720 Chemistry – Which Air Matters. *Atmos. Chem. Phys*., 17(14), 9081-9102, doi: 10.5194/acp-17-
721 9081-2017.
722
723 Prather, M.J., & J.C. Hsu (2019). A round Earth for climate models. *Proceedings of the National*
724 *Academy of Sciences*, 116 (39) 19330-19335; https://doi.org/10.1073/pnas.1908198116.
725
726 Séférian, R., Baek, S., Boucher, O., Dufresne, J.-L., Decharme, B., Saint-Martin, D., & Roehrig,
727 R (2016). An interactive ocean surface albedo scheme (OSAv1.0): formulation and evaluation in
728 ARPEGE-Climat (V6.1) and LMDZ (V5A). *Geoscientific Model Development*, 11, 321–338,
729 https://doi.org/10.5194/gmd-11-321-2018, 2018.
730
731 Søvde, O.A., M. J. Prather, I. S. A. Isaksen, T. K. Berntsen, F. Stordal, X. Zhu, C. D. Holmes, &
732 J. Hsu (2012). The chemical transport model Oslo CTM3. *Geoscientific Model Development*, 5,
733 1441-1469, doi:10.5194/gmd-5-1441-2012.
734

735 Spurr, R. & V.Natraj (2011). A linearized two-stream radiative transfer code for fast
736 approximation of multiple-scatter fields, *Journal of Quantitative Spectropscoy*, 112(2011)2630–
737 2637.
738
739 Thornberry, T. D., A. W. Rollins,M. A. Avery, S. Woods, R. P. Lawson,T. V. Bui, & R.-S. Gao
740 (2017). Ice water content-extinction relationships and effective diameter for TTL cirrus derived
741 from in situ measurements during ATTREX 2014. *Journal of geophysical Research-*
742 *Atmospheres*.,122, 4494–4507, doi:10.1002/2016JD025948.
743
744 Tompkins, A. M. & F. Di Giuseppe (2015). An Interpretation of Cloud Overlap Statistics.
745 *Journal of the Atmospheric Sciences*, 72(8), 2877-2889.
746
747 Tompkins, A.M. & F. Di Giuseppe (2007). Generalizing cloud overlap treatment to include
748 solar zenith angle effects on cloud geometry. *Journal of Atmospheric Sciences*., 64, 2116–2125,
749 doi:10.1175/JAS3925.1
750
751 Wild, O., Zhu, X., & Prather, M. J. (2000). Fast-J: Accurate simulation of in- and below-cloud
752 photolysis in tropospheric chemical models. *Journal of Atmospheric Chemistry*, 37(3), 245-282.
753
754 Wiscombe, W. J. (1977). Delta-M Method - Rapid yet Accurate Radiative Flux Calculations for
755 Strongly Asymmetric Phase Functions. *Journal of the Atmospheric Sciences*, 34(9), 1408-1422.
756
757 Wood, R. (2012). Stratocumulus Clouds. *Monthly Weather Rev*iew, 140, 2373–2423.
758
759 Yang, P., Hioki, S., Saito, M., Kuo, C. P., Baum, B. A., & Liou, K. N. (2018). A Review of Ice
760 Cloud Optical Property Models for Passive Satellite Remote Sensing. *Atmosphere*, 9(12).
761